Plasma cell but not CD20-mediated B cell depletion protects from bleomycin-induced lung fibrosis

Cecilia M Prêle[1,2,*], Tylah Miles[1,*], David R Pearce[3], Robert J O'Donoghue[4], Chris Grainge[5,6], Lucy Barrett[1], Kimberly Birnie[1], Andrew D Lucas[1], Svetlana Baltic[1], Matthias Ernst[7], Catherine Rinaldi[8], Geoffrey J Laurent[1,2], Darryl A Knight[9], Mark Fear[1,5], Gerard Hoyne[1,9], Robin J McAnulty[3,#] and Steven E Mutsaers[1,2,#]

[1]Institute for Respiratory Health, The University of Western Australia, Nedlands WA Australia; [2]Centre for Cell Therapy and Regenerative Medicine, School of Biomedical Sciences, The University of Western Australia, Nedlands WA Australia; [3]Centre for Inflammation and Tissue Repair, Division of Medicine, University College London, London UK; [4]Department of Pharmacology and Therapeutics, University of Melbourne, VIC Australia; [5]Centre for Healthy Lungs, Hunter Medical Research Institute, University of Newcastle, Newcastle, NSW, Australia; [6]Dept of Respiratory and Sleep Medicine, John Hunter Hospital, Newcastle, NSW, Australia; [7]Olivia Newton John Cancer Research Institute and La Trobe University School of Cancer Medicine, Heidelberg, VIC Australia; [8]Centre for Microscopy Characterisation and Analysis, The University of Western Australia, Nedlands WA Australia; [9]Providence Health Care Research Institute, Vancouver, BC, Canada; [10]Burn Injury Research Unit, School of Biomedical Sciences, The University of Western Australia, Nedlands WA Australia; [11]The University of Notre Dame Australia, Fremantle WA Australia.

Corresponding Author: Associate Professor Steven Mutsaers, Institute for Respiratory Health, QQ Block, QEII Medical Centre, 6 Verdun St, Nedlands 6009, WA, Australia.

Telephone: +61 (0)8 6151 0891; Email: steven.mutsaers@uwa.edu.au

Running Title: B cells in pulmonary fibrosis

Keywords: B cells, lung, transgenic/knockout mice, plasmablasts, plasma cells

Take home summary

Mice genetically depleted in B cells are protected from bleomycin-induced lung fibrosis but anti-CD20 treatment did not inhibit fibrosis, possibly due to retention of plasma cells (PC). PCs are abundant in IPF lung and selective depletion of PCs using bortezumib reduced Blm-induced lung fibrosis, suggesting PCs are potential targets for IPF therapy.

Footnote. This work is funded by NHMRC Project Grant #1067511 and British Lung Foundation Grant PPRG15-10. CMP, MF and SEM are supported by NHMRC Project Grant #1127337. Ms Tylah Miles is supported by a UWA Research Training Postgraduate Award and the Lung Foundation Australia Bill van Nierop PhD Scholarship. *CMP and TM have contributed equally to this work and share first authorship. # SEM and RJM have contributed equally to this work and share senior authorship.

Abstract

Idiopathic pulmonary fibrosis (IPF) is an interstitial lung disease associated with chronic inflammation and tissue remodelling leading to fibrosis, reduced pulmonary function, respiratory failure and death. Bleomycin (Blm)-induced lung fibrosis in mice replicates several clinical features of human IPF, including prominent lymphoid aggregates of predominantly B cells that accumulate in the lung adjacent to areas of active fibrosis. We have previously shown a requirement for B cells in the development of Blm-induced lung fibrosis in mice. To determine the therapeutic potential of inhibiting B cell function in pulmonary fibrosis, we examined the effects of anti-CD20 B-cell ablation therapy to selectively remove mature B cells from the immune system and inhibit Blm-induced lung fibrosis. Anti-CD20-B cell ablation did not reduce fibrosis in this model, however immune phenotyping of peripheral blood and lung resident cells revealed that anti-CD20 treated mice retained a high frequency of $CD19^+$ $CD138^+$ plasma cells (PCs). Interestingly, high levels of $CD138^+$ cells were also identified in the lung tissue of patients with IPF, consistent with the mouse model. Treatment of mice with bortezomib, which depletes PCs, reduced the level of Blm-induced lung fibrosis, implicating PCs as important effector cells in the development and progression of pulmonary fibrosis.

Introduction

Idiopathic pulmonary fibrosis (IPF) is an aggressive interstitial lung disease (ILD) characterised by excessive extracellular matrix (ECM) deposition and a chronic, progressive decline in lung function leading to death (1). Recent advances from genome-wide association studies have highlighted the significant role of epithelial dysfunction in the pathogenesis of IPF, however there remain limited treatment options with minimal impact on survival time for IPF patients (2). While several loci associated with epithelial function, including *MUC5B*, *TERT* and *TERC*, are thought to underpin the development of IPF (3), the variable progression of disease between patients with identical gene variants illustrates the complexity of IPF pathogenesis.

There is growing evidence that suggests a significant role for immune cells in the pathogenesis of IPF (4, 5). Lung tissue of IPF patients often display prominent lymphoid aggregates composed of T cells, B cells, macrophages and dendritic cells (6, 7). A subset of IPF patients present with serum autoantibodies, suggesting a breakdown in immune tolerance to either systemic (e.g. DNA or RNA) or lung-specific autoantigens that may be derived from damaged or dying lung epithelial cells (8-11). Fibrosis is not unique to IPF, as it is observed in a range of other connective tissue diseases including systemic lupus erythematosus (SLE), systemic sclerosis (SSc), Sjogren's syndrome and rheumatoid arthritis (RA) (12). These diseases share similar immune pathologies with IPF (13-15), suggesting that a breakdown in immune regulation plays an important role in the pathogenesis of lung fibrosis (7, 16, 17).

Mature B cells normally reside within lymphoid follicles of secondary lymphoid organs where they coordinate antibody synthesis in response to antigen (18). Several different B cell subsets exist within the immune system including naïve and memory cells and effector cells that can be short lived antibody secreting plasmablasts or long lived plasma cells (PCs) (19, 20). Long lived PCs are

now thought to hone to specific areas of the bone marrow, producing low levels of antibody for an indeterminate period of time and ramping up production if they encounter antigen, in addition to the rapid reactivation of memory B cells in the spleen, lymph nodes that can recirculate in peripheral blood (21). PCs are derived from activated, proliferating B cells (22), typically requiring B cell receptor (BCR) stimulation and signals from $CD4^+$ T helper cells in a T-dependent immune response, or BCR with Toll-like receptor stimulation plus cytokines from accessory cells in T-independent responses (23, 24).

Two additional B cell populations are B1 cells that localise to the peritoneal and pleural cavities, and marginal zone B cells (MZB) of the spleen. Both these B cell populations display innate-like properties that produce low affinity "natural" IgM antibodies against microbial antigens (25, 26). B1 cells are important for regulating tissue homeostasis through the recognition and clearance of apoptotic cells that can express self-antigens (27). A failure to clear cellular debris or dying cells can potentially drive inflammation and autoimmunity (28). B and T cells can also be recruited to peripheral tissues in response to infection or chronic immune stimulation, where they form tertiary lymphoid structures. These aggregates are organised similar to secondary lymphoid tissues consisting of B cell follicles, in which germinal centres can develop, and T cell areas that harbour antigen presenting cells (29).

We have demonstrated that in bleomycin (Blm)-induced pulmonary fibrosis, B cell dominant foci develop in the fibrotic lung tissue within 28 days (5, 30) and that mice lacking T and B cells or mature B cells only, were both protected from Blm-induced lung fibrosis (30, 31). However, these studies did not identify the B cell subset(s) that may be involved in this process.

In this study we provide evidence that in both mice and humans, $CD20^+$ B cells accumulate in prominent foci in the lung adjacent to areas of tissue fibrosis. However, depletion of $CD20^+$ B cells

failed to protect mice from Blm-induced pulmonary fibrosis. Importantly, $CD19^+$ $CD138^+$ PCs accumulated in significant numbers within the fibrotic lung which were not significantly affected by anti-CD20 antibody treatment. Furthermore, we identified a subset of IPF patients with a high proportion of plasmablasts in the blood and PCs in lung tissue, which were localised to discrete foci adjacent to fibrotic tissue. Depletion of lung PCs in mice using bortezomib significantly reduced the level of Blm-induced lung fibrosis. Our findings that both IPF and fibrotic mouse lung share similarities in the types of immune cell subsets that aggregate within the lung, and that PC ablation significantly inhibits Blm-induced lung fibrosis, suggests that PCs play a significant role in the pathogenesis of lung fibrosis and are a target for ablation therapy

Materials and Methods

Bleomycin-induced lung fibrosis. Mouse studies were approved by the University of Western Australia Animal Ethics Committee (AEC: RA/3/100/1339 and RA/3/100/1722), Austin Health Animal Ethics Committee (Ethics approval ID 2015-05305 and 2016-05320) and University College London Animal Care Committee under Home Office Licence in accordance with the United Kingdom Animals (Scientific Procedures) Act 1986. Male 10-12 week wild-type (wt) C57Bl/6J mice were used in this study. Bleomycin sulphate (Blm) (Hospira, Melbourne, VIC, Australia) or saline (0.9 %, Baxter, Old Toongabbie, NSW, Australia) was administered oropharangeally (1 mg/kg) unless otherwise stated. Blm-induced weight loss occurred in all animals with $\leq 10\%$ euthanised as they reached the 20% weight loss ethical limit. A minimum of four animals per group were used for end point quantitative analysis.

Anti-CD20 B cell depletion. Anti-CD20 antibody (donated by Genentech, South San Francisco, CA, USA) or isotype control IgG2a (Thermo Fisher Scientific, Scoresby, VIC, Australia, Cat#02-6200; 5 mg/kg) were administered i.p. either seven days before and seven days after Blm-treatment (prophylactic treatment) or on days 10 and 19 post-Blm treatment (therapeutic treatment). Blood,

spleen and lung tissue samples were collected for cell isolation (Supplementary results) and flow cytometric analysis (Supplementary results) performed using a B cell flow cytometry antibody screening panel (Supplementary table 1): mature follicular B cells ($CD45.2^+CD19^+CD20^+$), B1 regulatory B cells ($CD45.2^+CD5^+CD19^+$), plasma cells ($CD45.2^+CD19^+CD38^+CD138^+$), plasmablasts ($CD45.2^+CD19^+CD20^+CD138^-CD43^+CD38^+CD27^+$). In addition, lung tissue samples were weighed and snap frozen for HPLC analysis of hydroxyproline (30). For histological analysis, lungs were inflated and fixed in 4% paraformaldehyde (PFA) and processed for paraffin embedding. Tissue sections (3-5 μm) were stained with Masson's Trichrome or Martius Scarlet Blue using a Tissue-Tek DRS autostainer (Sakura, Japan) and slides scanned on a Nanozoomer HT slide scanner (Hamamatsu, Japan) and images exported with NDP.View2.

Bortezomib plasma cell depletion. Bortezomib stock solutions were prepared at 12.5 mg/mL in DMSO and stored at -80°C in single use aliquots. Bortezomib was prepared immediately prior to injection and administered at 1 mg/kg in 2% DMSO, 30% PEG300 i.p. twice a week beginning seven days before Blm treatment (day -7) until day 28 post Blm treatment. Vehicle only (2% DMSO, 30% PEG300) was administered i.p. to control animals. Blm (2 mg/kg), was administered intranasally on day 0. The mice were euthanised 28 days later and lungs inflated and fixed for *ex vivo* μCT quantification of fibrosis.

***Ex vivo* micro-computed tomography (μCT) analysis of lung fibrosis.** Lungs were inflated and fixed with 4% PFA, dried with hexamethyldisilazane (HMDS, Alfa Aesar, MA, USA) and CT scanned with a SkyScan 1172 (Bruker-MicroCT, Kontich, Belgium) with 12.6 μm pixel size as previously described (32). Reconstructed images were segmented with InForm image analysis software (Perkin-Elmer, MS, USA) to exclude background and to segment lungs into normal (green), fibrotic (blue) and airway regions. Data is either represented as percentage volume of fibrosis or sum pixel intensity, as a measure of lung density.

HPLC quantification of lung collagen. Following μCT or snap freezing, lung tissue was hydrolysed in 6 M HCl, amino acids purified and derivitised with 7-chloro-4-nitrobenzo-oxao-1,3-diazole (NBD-Cl, Acros Organics) and hydroxyproline levels measured by reverse-phase HPLC (Agilent 1100, LiChrospher column) as previously described (33). Hydroxyproline content was quantified against a known standard and pro-collagen content of samples calculated.

Histochemical and immunohistochemical analysis of fibrosis and immune cell infiltration in tissue. The expression and distribution of the T cell marker CD3, mouse pan B cell marker B220, B cell marker CD19, plasma cell, B cell precursor and some epithelial cell marker CD138 (syndecan-1; expresses weak epithelial cell staining) and B-1α cell and T cell marker CD5 on cells within lung and spleen tissue was determined by immunohistochemistry following a heat based citrate buffer method of antigen retrieval as previously described (30). A minimum of three tissue sections from different levels of the lung in at least three animals were examined for each study. For some immunohistochemistry studies, serial sections were prepared from area of lung examined.

IPF patient samples and age-matched controls. Serum samples from IPF patients (n=20, male=14, mean age 72.6±7.0 yrs, median age 73) and age-matched controls (n=17, male=10, mean age 66.2±9.4 yrs, median age 66) were collected in accordance with National Health and Medical Research Council guidelines and with ethics approval (Belberry Application Number HREC2011-10-497). Analysis of B cell activating factor (BAFF), APRIL and CXCL13 levels in IPF and control serum was performed using ProcartaPlex kits (Jomar Life Research, Scoresby, VIC, Australia) and measured on the Luminex 200 (R&D systems, Minneapolis, MN, USA). White blood cells collected from IPF (n=54, male=15, mean age 73.1±6.7 yrs, median age 73) and age-matched controls (n=26, male=5, mean age 69.5±10.3 yrs, median age 68) were analysed by flow cytometry in accordance with ethics approval Belberry Application Number HREC 2011-10-497, Newcastle,

New South Wales 2018/00207 and the University of Western Australia RA/4/20/5342. Fibrotic lung tissue was obtained from patients undergoing surgical lung biopsy or transplant surgery. All tissue was obtained with appropriate informed consent and its use approved by the East Midlands – Nottingham 2 NRES Committee, Ref. No. 12/EM/0058.

Statistical analysis. Experiments with two sample groups were analysed using an unpaired student T-test or Mann Whitney U test if the differences between two independent samples are not normally distributed. Experiments with more than two groups were analysed using a one-way ANOVA with post-hoc Tukey test for multiple comparisons. A p value <0.05 was considered significant.

Results

B cells aggregate in the lungs of Blm treated mice. In order to assess how Blm triggers B cell accumulation in the lung, we evaluated B cell numbers in the lung and circulation of wt mice by immunohistochemistry and flow cytometry. Tissue sections were stained with MSB to demonstrate the extent of fibrosis, with collagen shown in blue. In addition, sections of lung tissue were stained with the pan B cell antibody B220 which binds to the CD45 receptor expressed on mature B cells. Peripheral blood B cells were stained and analysed by flow cytometry using additional cell surface markers CD19 and CD20 which are expressed by mature B cells. We hypothesised that B cell numbers would initially increase in the circulation and then accumulate within the lung tissue. Immunohistochemical analysis of sections of C57Bl/6J mouse lung tissue at the peak of fibrosis, 28 days after Blm treatment, demonstrated an accumulation of multiple $B220^+$ B cell foci (Figure 1A iv, arrows and viii) compared to saline-treated controls. (Figure 1A ii, vi). Flow cytometry did not show any significant difference in circulating $CD19^+$ B cells in mice at either 7 days (Figure 1B) or 28 days after Blm treatment (Figure 1C). We expected to see an increase in B cells in the lung from day 7 to 28, however there was no significant change (Figure 1B and C).

Blm-induced collagen deposition is refractory to anti-CD20-mediated ablation of mature B cells. To determine if anti-CD20-mediated depletion of mature B cells protected Blm treated mice from fibrosis, wt mice received prophylactic treatment comprising two doses of anti-CD20 antibody or an isotype control IgG2a antibody 7 days before and 7 days after Blm treatment (Figure 2). Flow cytometry demonstrated almost a complete depletion of circulating $CD19^+$ B cells, CD19 is a pan-B cell marker expressed on all B cells, on day 7 (prior to the second anti-CD20 antibody dose) and 28 days post-Blm treatment (Figure 2A). Immunohistochemistry and flow cytometry also showed a decrease in the number of $B220^+$ cells in sections of spleen tissue (Figure 2B) and $CD19^+$ cells from dissociated lung tissue (Figure 2C) of anti-CD20 antibody treated mice compared with mice treated with the IgG2a isotype control antibody. However, anti-CD20 treatment did not show any significant change in fibrosis as determined by μCT and HPLC-assessed collagen deposition compared to mice that received the isotype control (Figures 2D-F). To determine if the timing of B cell depletion influences the fibrotic response, anti-CD20 antibodies were administered on days 10 and 19 post-Blm treatment. However, there was still no change in fibrosis compared with control (Figure 2G).

$CD138^+$ plasma cells and $CD5^+$ cells were increased in the circulation and lungs of Blm treated mice. Anti-CD20 antibody-mediated B cell ablation prior to Blm treatment was not sufficient to reduce fibrosis. Therefore, we examined the different B cell populations in wt C57BL/6 mice in response to saline or Blm treatment alone using flow cytometry and immunohistochemistry and compared them with saline controls. In Blm only treated mice, there was no change in the frequency of CD19+ CD38+ plasmablasts in blood or $CD19^+$ $CD138^+$ plasma B cells in lung or $CD5^+$ $CD19^+$ B cells within the circulation or lung at day 7 or 28 compared with saline control (Figures 3A-D). However, immunostaining demonstrated the formation of aggregates of $B220^+$, $CD19^+$, $CD138^+$ and $CD3^+$ cells in Blm-treated mouse lung (Figure 3E and F).

We then examined the lymphocyte subsets of wt mice treated with saline or Blm only or those that received Blm with anti-CD20 treatment or an isotype control. Anti-CD20 depletion prior to Blm markedly reduced the number of $B220^+$ cells within the lung (Figure 4A) and significantly reduced the number of $CD19^+$ lymphocytes within the circulation (Figure 4B) of mice 28 days post Blm treatment. An increase in the proportion of $CD5^+$ cells was detected within the lungs of anti CD20 antibody treated mice (Figure 4A). Subsequent flow cytometry analysis of dissociated lung tissue showed that was due to a significant increase in $CD5^+CD3^+$ T cells but not $CD5^+CD19^+$ B cells excluding the possibility of expansion of CD5+ B1 cells in the lung (Figure 4B). In addition, a significant increase in PC number was detected in anti-CD20 antibody treated mice compared to IgG2a control (Figure 4C). These data suggest that while prophylactic anti-CD20 depletion successfully targeted CD20 expressing B cells, there were a large number of PCs that remained in the lung following Blm treatment and may have contributed to the lung fibrosis.

Plasma cell depletion inhibited lung fibrosis. To investigate a role for PCs in lung fibrosis, we treated Blm exposed mice twice weekly with bortezomib, a selective inhibitor of the 26S proteasome that targets PCs and is used for the treatment of multiple myeloma and mantle-cell lymphoma. Mice treated with bortezomib showed a significant reduction in fibrosis as determined by µCT analysis (Figure 5A). Immunfluorescent staining of the lungs for CD138 expression showed almost complete absence of PCs in Bortezomib treated lungs (Figure 5B).

B cell accumulation in IPF. We then explored to what extent the mouse data corroborated with clinical data of B-cell accumulation in lung sections from IPF patients. Immunohistochemistry performed on IPF lung tissue showed an accumulation of $CD20^+$, $CD5^+$ and $CD138^+$ cells within regions of fibrosis (Figure 6A), consistent with observations in the lungs of Blm treated mice. The peripheral blood of IPF patients also contained a significant increase in plasmablasts compared with healthy controls (Figure 6B). To determine if plasmablast numbers are maintained in IPF patients,

four surviving IPF patients were rebled 18 months after their initial blood sample and plasmablast numbers assessed by flow cytometry. All four surviving IPF patients demonstrated an even higher proportion of plasmablasts in their blood compared to the primary bleed (Figure 5C and D).

Discussion

There is growing evidence that the immune system plays an important role in the pathobiology of a range of fibrotic diseases including IPF, SSc and liver fibrosis (4). Using a mouse model of Blm-induced lung fibrosis, we previously demonstrated that B cells were an important effector cell population in the regulation of lung fibrosis in mice (30). Genetic depletion of *Rag1* on a high STAT3 background blocked the formation of mature B and T cells and this was sufficient to protect the lungs of mice from Blm-induced fibrosis. Furthermore, genetic depletion of mature B cells in muMt$^{-/-}$ mice on a high STAT3 background and CD19$^{-/-}$ mice, which have reduced B cell activation, also reduced collagen synthesis and fibrosis following Blm treatment, specifically implicating mature B cells in lung fibrogenesis (30, 34). Yet an important question remained as to the identity of the B cell subset that might contribute to fibrotic disease.

To assess the implication of these genetic findings, we explored a more clinically relevant model of B cell depletion; mouse anti-CD20 antibody treatment, based on the human anti-CD20 antibody, rituximab. Here we reveal that antibody-mediated depletion of CD20^{+} B cells, which successfully removed ~95% of mature B cells from the peripheral circulation and tissues (35), did not prevent Blm-induced lung fibrosis. To resolve this discrepancy, we firstly demonstrated that antibody-mediated B cell depletion failed to remove all mature B cell populations. PCs downregulate CD20 during their differentiation making them resistant to antibody depletion, allowing their retention in the blood and peripheral tissues. However, PCs have been implicated in autoimmune diseases such as SLE, vasculitis and Sjrogens syndrome through the production of self-reactive antibodies to either host proteins or nucleic acids (19, 36).

Several studies have shown that IPF patients have increased plasmablasts compared to controls (4, 37, 38). Furthermore, proteomic analysis on IPF lung tissue demonstrated an accumulation of MZB-1 positive B cells that were characterised as $CD20^{-}CD138^{+}CD38^{+}CD27^{+}$ (39), which share a number of phenotypic properties with conventional PCs. Groot Kormelink and colleagues also showed that PCs and activated mast cells accumulate in the lung tissue of patients with IPF and hypersensitivity pneumonitis (40). Interestingly, one study using single cell RNA sequencing data did not show a significant increase in PCs or plasmablasts in IPF but it was unclear what criteria was used to catagorise these cells (41). In this study we confirmed the presence of PCs and plasmablasts in the lung and blood of IPF patients respectively, and showed that plasmablasts were increased in a subpopulation of IPF patients compared with controls, consistent with other studies.

Plasmablasts are PC precursors derived from the differentiation of activated memory B cells generated in response to antigen exposure. Plasmablasts are short lived antibody secreting effector cells in the immune system and exhibit a transient presence in the peripheral blood during their transit from secondary lymphoid tissues (e.g. lymph node or spleen) to the bone marrow, where they can give rise to long lived PCs. Currently there is little known about the origin and persistence of B cell subsets in IPF patients. To begin to address this issue we rebled four surviving IPF patients 18 months after their initial blood sample and the second sample was analysed by flow cytometry. All four IPF patients displayed even higher proportion of plasmablasts in the blood compared to the primary bleed, suggesting that these patients must experience ongoing immune responses that could be in response to exposure to environmental antigens or self-antigens.

Rituximab is a human anti-CD20 antibody that has been used clinically to deplete B cells in autoimmune diseases and different types of haematological cancers (42-44). Rituximab has also

been used in clinical trials for SSc, non IPF ILDs and IPF exacerbations (45-47) with mixed results and limited improvement in lung function. Rituximab reduced recall responses to some antigens in lymphoma and RA patients but total immunoglobulin (Ig) levels in patients remained unchanged (48). Therefore, if PCs have a role in the pathobiology of IPF, the use of rituximab for immunotherapy may be limited. DiLillo et al. revealed that anti-CD20 antibody treatment in wt mice depleted natural and antigen-induced IgM responses and memory B cell populations but had no effect on the number of long-lived PCs in bone marrow, nor the total serum Ig levels or the titres of antigen-specific antibodies (43). Treatment of adult autoimmune tight skin mice, a genetic model of SSc, with anti-CD20, did not affect skin fibrosis or autoantibody levels with established disease, however continuous delivery of anti-CD20 to young neonatal tight skin mice prior to disease onset reduced skin fibrosis and autoantibody production (35). PCs are resistant to elimination by the anti-CD20 antibody because they lack expression of the target antigen. Therefore PC targeted therapies are required to treat autoimmune diseases or cancers like multiple myeloma (MM), a leukaemia of PCs. Monoclonal antibody therapies are currently used in clinical practice to target other PC surface markers including signalling lymphocyte activation molecule F7 (SlamF7) and CD38 (49, 50), while the proteasome inhibitor bortezomib is an anti-cancer therapy used in the treatment of MM, but toxicity and off-target effects are common (51).

The function of the proteasome is critically important in PCs because of their high rate of antibody synthesis. Proteasome inhibition in PCs causes accumulation of defective immunoglobulins and misfolded proteins, resulting in PC death (52-54). Proteosome inhibitors have been shown to ameliorate symptoms in patients with autoimmune diseases including SLE, RA, myasthenia gravis, neuromyelitis optica spectrum disorder, chronic inflammatory demyelinating polyneuropathy and autoimmune hematologic diseases that were unresponsive to conventional therapies (55). Bortezomib has previously been shown to significantly reduce lung fibrosis in Blm treated mice in two other studies, although it was suggested its effects were through inhibition of transforming

growth factor beta signalling (56) or by modulating fibroblast function independent of proteasome inhibition (57). In this study we confirmed that bortezomib reduced lung fibrosis in Blm treated mice but also showed almost complete depletion of PCs in bortezomib treated lung tissue. Although we cannot conclude that the effects of bortezomib are solely due to PC depletion, the observation that genetic depletion of mature B cells in $Rag^{-/-}$and $muMT^{-/-}$ mice (30) and reduced B cell activation in $CD19^{-/-}$ mice, which all inhibit PC function, block Blm-induced lung fibrosis, yet CD20 depletion which does not inhibit PC function doesn't inhibit fibrosis, strongly supports a role for PCs in the development of lung fibrosis.

In conclusion, this study provides new evidence supporting the role of PCs and plasmablasts in Blm-induced lung fibrosis, and importantly, for their accumulation in the lungs of clinically diagnosed IPF patients. The results presented here have important implications in our understanding of B cell subsets in pulmonary fibrosis and for the consideration of future therapies in IPF. It will be important to determine whether there is clonal expansion of particular PCs and to identify antigen specificity of antibodies produced by PCs in IPF patients to elucidate their role in tissue damage and whether they are directed to self or foreign antigens. Resolving these issues may help guide the development and use of immune therapies in IPF.

Figure Legends

Figure 1. B cells are a prominent feature in Blm-induced pulmonary fibrosis in mice **a)** Immunohistochemical analysis of B220 staining 28 days post oropharyngeal Blm treatment reveals an increase in $B220^{+}$ cells (iv, arrows and viii) at sites of fibrosis (Martius Scarlet Blue [MSB] staining, iii, vii collagen blue) compared to saline treated controls (MSB i, v) and B220 stained (ii, vii). Images i-iv represent low magnification, scale bar = 200 μm. Images v-iv represent high magnification, scale bar = 100 μm. Images are representative of three mice in each group. **b)** Flow cytometry did not show a significant increase in circulating or lung resident $CD45.2^{+}$ $CD19^{+}$ B cells

in Blm treated mice 7 days post treatment (n≥4). **c)** No significant difference in circulating $CD45.2^+$ $CD19^+$ B cells was detected in isolated PBMCs 28 days following Blm treatment. There was no significant difference in the number of $CD19^+$ cells detected in dissociated lung tissue post-Blm treatment. Statistical analysis was performed using an unpaired student t-test (n≥10), * $p \leq 0.05$.

Figure 2. Anti-CD20-mediated B cell depletion does not protect mice against oropharyngeal Blm-induced pulmonary fibrosis**. a)** Anti-CD20 therapy 7 days prior to and 7 days following Blm successfully reduced circulating $CD19^+$ cells as measured by flow cytometry in mice on day 7 and 28 post Blm treatment (n≥4). **b)** Immunohistochemical analysis of B220 expression on spleen tissue sections demonstrated a marked decrease in $B220^+$ cell numbers in anti-CD20-treated mice compared to IgG2a-treated control mice. Scale bars = 100 µm and 25 µm for higher power. **c)** Quantitative flow cytometry analysis showed that anti-CD20 treatment significantly reduced Blm-induced $CD19^+$ cell numbers in the lung on day 7 and day 28 (n≥4). **d)** Masson's trichrome staining showed no overt difference in the extent of collagen deposition (blue) in mice treated with Blm and anti-CD20 compared to Blm only and mice treated with Blm and IgG2a. Scale bars = 200 µm. **e-g)** Quantitative analysis of fibrosis and collagen deposition was performed by µCT and HPLC analysis of hydroxyproline but there was no significant difference in mice treated with Blm and anti-CD20 compared with Blm and vehicle control. **e)** Represents a preventative model where anti-CD20 was administered 7 days prior to, and 7 days after Blm treatment. µCT analysis was performed *ex vivo* and the lung density was used as a representation of fibrosis. There was no difference in the amount of Blm-induced fibrosis in IgG2a or αCD20 treated mice (n≥7). **f)** HPLC analysis did not show any difference in the amount of Blm-induced lung collagen in in IgG2a or αCD20 treated mice confirming that αCD20 had no effect on lung fibrosis (n≥6). **g)** The data represents a therapeutic model where anti-CD20 was administered on days 10 and 19 post-Blm treatment. Similarly, there was no detectable change in the amount of collagen in the lungs of Blm and anti-CD20 treated mice

compared to Blm alone or Blm and IgG2a treated mice (HPLC n≥5 and μCT n≥6). All images are representative of at least three mice per group. * $p \leq 0.05$, **$p \leq 0.005$, ***$p \leq 0.0005$, ****$p \leq 0.0001$.

Figure 3. Characterisation of specific B cell subsets in the peripheral circulation and lung of mice following oropharyngeal Blm-induced pulmonary fibrosis. **a)** Blm treatment had no effect on the number of $CD5^+$ $CD19^+$ B cells or $CD19^+CD38^+CD138^+$ PCs detected in PBMCs on day 7 post Blm treatment (n≥6) or **b)** $CD5^+CD19^+$ B cells or $CD19^+CD138^+$ PCs in the lung 7 days post Blm treatment (n≥4). **c-d)** No significant difference was observed in the frequency of $CD19^+CD138^+$ PCs in the circulation or the lung at day 28 post Blm treatment (n≥6). No significant increase in $CD5^+CD19^+$ cells was observed in the lung 28 days post Blm treatment (n≥6). Statistical analysis was performed using an unpaired student t-test, * $p \leq 0.05$. **e)** Mouse lung tissue from saline treated or Blm treated mice (day 28) was stained with Martius Scarlet Blue (MSB; collagen blue) or with anti-B220 antibody. $B220^+$ cell aggregates were detected in the lungs of Blm treated mice (brown DAB staining). **f)** Serial sections of Blm treated lung stained with Masson's Trichrome (MT) and immune markers. $CD3^+$ lymphocytes, $CD19^+$ B cells and $CD138^+$ plasma cells were detected at sites of fibrosis. All images are representative of at least three mice per group. Scale bars = 50 μm.

Figure 4. B cell composition of the lungs of mice following anti-CD20 and Blm treatment. **a)** Mouse lung tissue from Blm exposed mice treated with anti-CD20 or isotype control (day 28) was stained with Masson's Trichrome (collagen blue). Immunohistochemistry shows a marked reduction in $B220^+$ B cells in 28 day treated mice and retention of $CD5^+$ expressing cells compared with mice treated with Blm and IgG2a. All images are representative of at least three mice per group. Scale bars = 50 μm. b) Flow cytometry confirms depletion of $CD19^+$ cells in the circulation but revealed no increase in circulating $CD5^+$ B cells, but a significant increase in CD5+ T cells following anti-CD20 depletion (n≥4). **c)** However, anti-CD20 treatment did not deplete the plasma

cell population in the lung 28 days following Blm (n≥5). Statistical analysis was performed using a one-way ANOVA, * $p \leq 0.05$, **$p \leq 0.005$, ***$p \leq 0.0005$, ****$p \leq 0.0001$, ns = not significant.

Figure 5. Plasma cell depletion reduces Blm-induced lung fibrosis. Mice were given either a vehicle control or bortezomib at day -7 and twice weekly until 28 days after intranasal Blm (2 mg/kg) treatment (day 0) and the volume of fibrosis was quantified by γCT analysis. a) Blm induced significant lung fibrosis compared to saline, which was reduced following bortezomib treatment (n≥4). **b)** Immunofluorescence staining of lung tissue from Blm + vehicle or bortezomib-treated mice was performed to detect PCs within the lungs. The nuclei are stained blue, $CD19^+$ cells are stained red and $CD138^+$ cells are stained green. The PCs are positive for both CD19 and CD138. Some epithelial cell staining is seen in the bortezomib treated group. The figure shows a representative image from each group (n≥4). *$p<0.05$. A lower power image showing an extensive area of fibrosis is shown in Supplementary Figure 3.

Figure 6. Analysis of B cell populations in the lung and peripheral blood of IPF patients and aged matched healthy controls. **a)** Martius scarlet blue (MSB) stained and anti-CD20 stained sections of IPF lung tissue demonstrate collagen deposition (blue) and an accumulation of $CD20^+$ B cells within regions of fibrosis (brown). In addition, $CD5^+$ and $CD138^+$ PCs were abundant in IPF lung tissue. All images are representative of at least three mice per group. Scale bars = 50 μm. b) Quantitation of the frequency of plasmablasts and memory B cells in white blood cells of healthy controls (n=27) and IPF patients (n=51) as determined by flow cytometry. Each symbol represents the value from one individual. c) Representative dot plot and contour plots of $CD19^+$ $CD20^+$ B cells from an IPF patient that was bled on two separate occasions 18 months apart. $CD19^+$ vs $CD20^+$ staining identifies mature B cells (top panel), $CD20^+CD27^+$ cells identifies memory B cells (middle panel) and $CD20^+$ $CD38^+$ identifies plasmablasts (bottom panel), n=4. d) The graph shows the

frequency of $CD19^{+}CD20^{+}$ $CD27^{+}$ $CD38^{+}$ plasmablasts in the peripheral blood of four different individuals bled on two occasions 18 months apart.

Acknowledgements

The authors would like to acknowledge the generosity of Genentech, USA for providing the anti-CD20 used in this study. In addition, we would like to thank Dr Chuan Bian Lim and Dr Joe Yasa for technical support and the Institute for Respiratory Health's Clinical Trial Unit for blood sample collection. We acknowledge the facilities and the scientific and technical assistance of the Australian Microscopy & Microanalysis Research Facility at the Centre for Microscopy, Characterisation & Analysis, University of Western Australia (UWA), a facility funded by the University, State and Commonwealth Governments. This study was supported by NHMRC grant # 1067511. Ms Tylah Miles is supported by a Research Training Program Scholarship from UWA and the Lung Foundation Australia Bill van Nierop PhD Scholarship.

Disclosure of interest

National Health & Medical Research Council (NHMRC) Project grants ID# APP1067511 SM, CP, RM, GL, GH, DK, RO, ME

British Lung Foundation Project grant No. PPRG15-10 RM, SM, CP, DP

Genentech, provided anti-CD20 antibody

UWA Research Training Program Scholarship and the Lung Foundation Australia Bill van Nierop PhD Scholarship, TM.

All other authors have nothing to disclose.

References

1. Lederer DJ, Martinez FJ. Idiopathic Pulmonary Fibrosis. N Engl J Med. 2018;378(19):1811-23.

2. Maher TM, Evans IC, Bottoms SE, Mercer PF, Thorley AJ, Nicholson AG, et al. Diminished prostaglandin E2 contributes to the apoptosis paradox in idiopathic pulmonary fibrosis. Am J Respir Crit Care Med. 2010;182(1):73-82.

3. Richeldi L, Collard HR, Jones MG. Idiopathic pulmonary fibrosis. Lancet. 2017;389(10082):1941-52.

4. Heukels P, van Hulst JAC, van Nimwegen M, Boorsma CE, Melgert BN, von der Thusen JH, et al. Enhanced Bruton's tyrosine kinase in B-cells and autoreactive IgA in patients with idiopathic pulmonary fibrosis. Respir Res. 2019;20(1):232.

5. Hoyne GF, Elliott H, Mutsaers SE, Prele CM. Idiopathic pulmonary fibrosis and a role for autoimmunity. Immunol Cell Biol. 2017;95(7):577-83.

6. Marchal-Somme J, Uzunhan Y, Marchand-Adam S, Valeyre D, Soumelis V, Crestani B, et al. Cutting edge: nonproliferating mature immune cells form a novel type of organized lymphoid structure in idiopathic pulmonary fibrosis. J Immunol. 2006;176(10):5735-9.

7. Todd NW, Scheraga RG, Galvin JR, Iacono AT, Britt EJ, Luzina IG, et al. Lymphocyte aggregates persist and accumulate in the lungs of patients with idiopathic pulmonary fibrosis. J Inflamm Res. 2013;6:63-70.

8. Dobashi N, Fujita J, Murota M, Ohtsuki Y, Yamadori I, Yoshinouchi T, et al. Elevation of anti-cytokeratin 18 antibody and circulating cytokeratin 18: anti-cytokeratin 18 antibody immune complexes in sera of patients with idiopathic pulmonary fibrosis. Lung. 2000;178(3):171-9.

9. Rioja I, Hughes FJ, Sharp CH, Warnock LC, Montgomery DS, Akil M, et al. Potential novel biomarkers of disease activity in rheumatoid arthritis patients: CXCL13, CCL23, transforming growth factor alpha, tumor necrosis factor receptor superfamily member 9, and macrophage colony-stimulating factor. Arthritis Rheum. 2008;58(8):2257-67.

10. Shum AK, Alimohammadi M, Tan CL, Cheng MH, Metzger TC, Law CS, et al. BPIFB1 is a lung-specific autoantigen associated with interstitial lung disease. Sci Transl Med. 2013;5(206):206ra139.

11. Shum AK, DeVoss J, Tan CL, Hou Y, Johannes K, O'Gorman CS, et al. Identification of an autoantigen demonstrates a link between interstitial lung disease and a defect in central tolerance. Sci Transl Med. 2009;1(9):9ra20.

12. Fischer A, du Bois R. Interstitial lung disease in connective tissue disorders. Lancet. 2012;380(9842):689-98.

13. Jonsson MV, Skarstein K, Jonsson R, Brun JG. Serological implications of germinal center-like structures in primary Sjogren's syndrome. J Rheumatol. 2007;34(10):2044-9.

14. Kogame T, Yamashita R, Hirata M, Kataoka TR, Kamido H, Ueshima C, et al. Analysis of possible structures of inducible skin-associated lymphoid tissue in lupus erythematosus profundus. J Dermatol. 2018;45(9):1117-21.

15. Takemura S, Braun A, Crowson C, Kurtin PJ, Cofield RH, O'Fallon WM, et al. Lymphoid neogenesis in rheumatoid synovitis. J Immunol. 2001;167(2):1072-80.

16. Wallace WA, Howie SE. Upregulation of tenascin and TGFbeta production in a type II alveolar epithelial cell line by antibody against a pulmonary auto-antigen. J Pathol. 2001;195(2):251-6.

17. Wallace WA, Roberts SN, Caldwell H, Thornton E, Greening AP, Lamb D, et al. Circulating antibodies to lung protein(s) in patients with cryptogenic fibrosing alveolitis. Thorax. 1994;49(3):218-24.

18. Cremasco V, Woodruff MC, Onder L, Cupovic J, Nieves-Bonilla JM, Schildberg FA, et al. B cell homeostasis and follicle confines are governed by fibroblastic reticular cells. Nat Immunol. 2014;15(10):973-81.

19. Hiepe F, Radbruch A. Plasma cells as an innovative target in autoimmune disease with renal manifestations. Nat Rev Nephrol. 2016;12(4):232-40.

20. Shapiro-Shelef M, Calame K. Regulation of plasma-cell development. Nat Rev Immunol. 2005;5(3):230-42.

21. Ionescu L, Urschel S. Memory B Cells and Long-lived Plasma Cells. Transplantation. 2019;103(5):890-8.

22. Nutt SL, Hodgkin PD, Tarlinton DM, Corcoran LM. The generation of antibody-secreting plasma cells. Nat Rev Immunol. 2015;15(3):160-71.

23. de Vinuesa CG, Cook MC, Ball J, Drew M, Sunners Y, Cascalho M, et al. Germinal centers without T cells. J Exp Med. 2000;191(3):485-94.

24. Sze DM, Toellner KM, Garcia de Vinuesa C, Taylor DR, MacLennan IC. Intrinsic constraint on plasmablast growth and extrinsic limits of plasma cell survival. J Exp Med. 2000;192(6):813-21.

25. Berland R, Wortis HH. Origins and functions of B-1 cells with notes on the role of CD5. Annu Rev Immunol. 2002;20:253-300.

26. Ehrenstein MR, Notley CA. The importance of natural IgM: scavenger, protector and regulator. Nat Rev Immunol. 2010;10(11):778-86.

27. Casciola-Rosen LA, Anhalt G, Rosen A. Autoantigens targeted in systemic lupus erythematosus are clustered in two populations of surface structures on apoptotic keratinocytes. J Exp Med. 1994;179(4):1317-30.

28. Peng Y, Kowalewski R, Kim S, Elkon KB. The role of IgM antibodies in the recognition and clearance of apoptotic cells. Mol Immunol. 2005;42(7):781-7.

29. Halle S, Dujardin HC, Bakocevic N, Fleige H, Danzer H, Willenzon S, et al. Induced bronchus-associated lymphoid tissue serves as a general priming site for T cells and is maintained by dendritic cells. J Exp Med. 2009;206(12):2593-601.

30. O'Donoghue RJ, Knight DA, Richards CD, Prele CM, Lau HL, Jarnicki AG, et al. Genetic partitioning of interleukin-6 signalling in mice dissociates Stat3 from Smad3-mediated lung fibrosis. EMBO Mol Med. 2012;4(9):939-51.

31. Prele CM, Yao E, O'Donoghue RJ, Mutsaers SE, Knight DA. STAT3: a central mediator of pulmonary fibrosis? Proc Am Thorac Soc. 2012;9(3):177-82.

32. Scotton CJ, Hayes B, Alexander R, Datta A, Forty EJ, Mercer PF, et al. Ex vivo micro-computed tomography analysis of bleomycin-induced lung fibrosis for preclinical drug evaluation. Eur Respir J. 2013;42(6):1633-45.

33. Mutsaers SE, Foster ML, Chambers RC, Laurent GJ, McAnulty RJ. Increased endothelin-1 and its localization during the development of bleomycin-induced pulmonary fibrosis in rats. Am J Respir Cell Mol Biol. 1998;18(5):611-9.

34. Komura K, Yanaba K, Horikawa M, Ogawa F, Fujimoto M, Tedder TF, et al. CD19 regulates the development of bleomycin-induced pulmonary fibrosis in a mouse model. Arthritis Rheum. 2008;58(11):3574-84.

35. Hasegawa M, Hamaguchi Y, Yanaba K, Bouaziz JD, Uchida J, Fujimoto M, et al. B-lymphocyte depletion reduces skin fibrosis and autoimmunity in the tight-skin mouse model for systemic sclerosis. Am J Pathol. 2006;169(3):954-66.

36. Chesi M, Bergsagel PL. Molecular pathogenesis of multiple myeloma: basic and clinical updates. Int J Hematol. 2013;97(3):313-23.

37. Li X, Huang Y, Ye N, He J. Analysis of immune-related genes in idiopathic pulmonary fibrosis based on bioinformatics and experimental verification. Ann Palliat Med. 2021;10(11):11598-614.

38. Xue J, Kass DJ, Bon J, Vuga L, Tan J, Csizmadia E, et al. Plasma B lymphocyte stimulator and B cell differentiation in idiopathic pulmonary fibrosis patients. J Immunol. 2013;191(5):2089-95.

39. Schiller HB, Mayr CH, Leuschner G, Strunz M, Staab-Weijnitz C, Preisendorfer S, et al. Deep Proteome Profiling Reveals Common Prevalence of MZB1-Positive Plasma B Cells in Human Lung and Skin Fibrosis. Am J Respir Crit Care Med. 2017;196(10):1298-310.

40. Groot Kormelink T, Pardo A, Knipping K, Buendia-Roldan I, Garcia-de-Alba C, Blokhuis BR, et al. Immunoglobulin free light chains are increased in hypersensitivity pneumonitis and idiopathic pulmonary fibrosis. PLoS One. 2011;6(9):e25392.

41. Adams TS, Schupp JC, Poli S, Ayaub EA, Neumark N, Ahangari F, et al. Single-cell RNA-seq reveals ectopic and aberrant lung-resident cell populations in idiopathic pulmonary fibrosis. Sci Adv. 2020;6(28):eaba1983.

42. Colombat P, Salles G, Brousse N, Eftekhari P, Soubeyran P, Delwail V, et al. Rituximab (anti-CD20 monoclonal antibody) as single first-line therapy for patients with follicular lymphoma with a low tumor burden: clinical and molecular evaluation. Blood. 2001;97(1):101-6.

43. DiLillo DJ, Hamaguchi Y, Ueda Y, Yang K, Uchida J, Haas KM, et al. Maintenance of long-lived plasma cells and serological memory despite mature and memory B cell depletion during CD20 immunotherapy in mice. J Immunol. 2008;180(1):361-71.

44. Reff ME, Carner K, Chambers KS, Chinn PC, Leonard JE, Raab R, et al. Depletion of B cells in vivo by a chimeric mouse human monoclonal antibody to CD20. Blood. 1994;83(2):435-45.

45. Daoussis D, Melissaropoulos K, Sakellaropoulos G, Antonopoulos I, Markatseli TE, Simopoulou T, et al. A multicenter, open-label, comparative study of B-cell depletion therapy with Rituximab for systemic sclerosis-associated interstitial lung disease. Semin Arthritis Rheum. 2017;46(5):625-31.

46. Donahoe M, Valentine VG, Chien N, Gibson KF, Raval JS, Saul M, et al. Autoantibody-Targeted Treatments for Acute Exacerbations of Idiopathic Pulmonary Fibrosis. PLoS One. 2015;10(6):e0127771.

47. Elhai M, Boubaya M, Distler O, Smith V, Matucci-Cerinic M, Alegre Sancho JJ, et al. Outcomes of patients with systemic sclerosis treated with rituximab in contemporary practice: a prospective cohort study. Ann Rheum Dis. 2019;78(7):979-87.

48. Cambridge G, Leandro MJ, Edwards JC, Ehrenstein MR, Salden M, Bodman-Smith M, et al. Serologic changes following B lymphocyte depletion therapy for rheumatoid arthritis. Arthritis Rheum. 2003;48(8):2146-54.

49. de Weers M, Tai YT, van der Veer MS, Bakker JM, Vink T, Jacobs DC, et al. Daratumumab, a novel therapeutic human CD38 monoclonal antibody, induces killing of multiple myeloma and other hematological tumors. J Immunol. 2011;186(3):1840-8.

50. Tai YT, Dillon M, Song W, Leiba M, Li XF, Burger P, et al. Anti-CS1 humanized monoclonal antibody HuLuc63 inhibits myeloma cell adhesion and induces antibody-dependent cellular cytotoxicity in the bone marrow milieu. Blood. 2008;112(4):1329-37.

51. Loke C, Mollee P, McPherson I, Walpole E, Yue M, Mutsando H, et al. Bortezomib use and outcomes for the treatment of multiple myeloma. Intern Med J. 2020.

52. Field-Smith A, Morgan GJ, Davies FE. Bortezomib (Velcadetrade mark) in the Treatment of Multiple Myeloma. Ther Clin Risk Manag. 2006;2(3):271-9.

53. Obeng EA, Carlson LM, Gutman DM, Harrington WJ, Jr., Lee KP, Boise LH. Proteasome inhibitors induce a terminal unfolded protein response in multiple myeloma cells. Blood. 2006;107(12):4907-16.

54. Wang J, Fang Y, Fan RA, Kirk CJ. Proteasome Inhibitors and Their Pharmacokinetics, Pharmacodynamics, and Metabolism. Int J Mol Sci. 2021;22(21):11595.

55. Khalesi N, Korani S, Korani M, Johnston TP, Sahebkar A. Bortezomib: a proteasome inhibitor for the treatment of autoimmune diseases. Inflammopharmacology. 2021;29(5):1291-306.

56. Mutlu GM, Budinger GR, Wu M, Lam AP, Zirk A, Rivera S, et al. Proteasomal inhibition after injury prevents fibrosis by modulating TGF-beta(1) signalling. Thorax. 2012;67(2):139-46.

57. Penke LRK, Speth J, Wettlaufer S, Draijer C, Peters-Golden M. Bortezomib Inhibits Lung Fibrosis and Fibroblast Activation without Proteasome Inhibition. Am J Respir Cell Mol Biol. 2021;66(1):23-37.

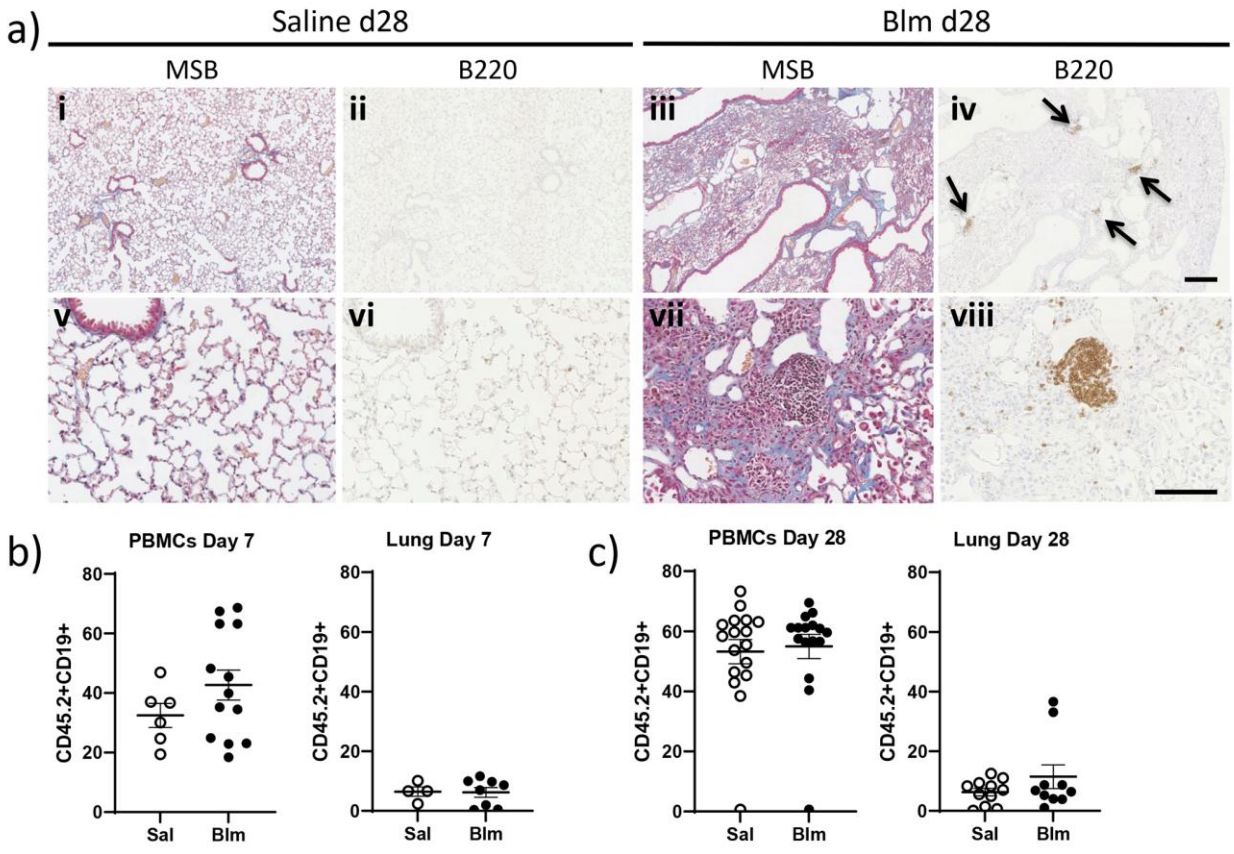
a)
Saline d28
Blm d28
MSB
B220
MSB
B220
i
ii
iii
iv
v
vi
vii
viii
b)
PBMCs Day 7
Lung Day 7
c)
PBMCs Day 28
Lung Day 28
CD45.2+CD19+
0
20
40
60
80
Sal
Blm

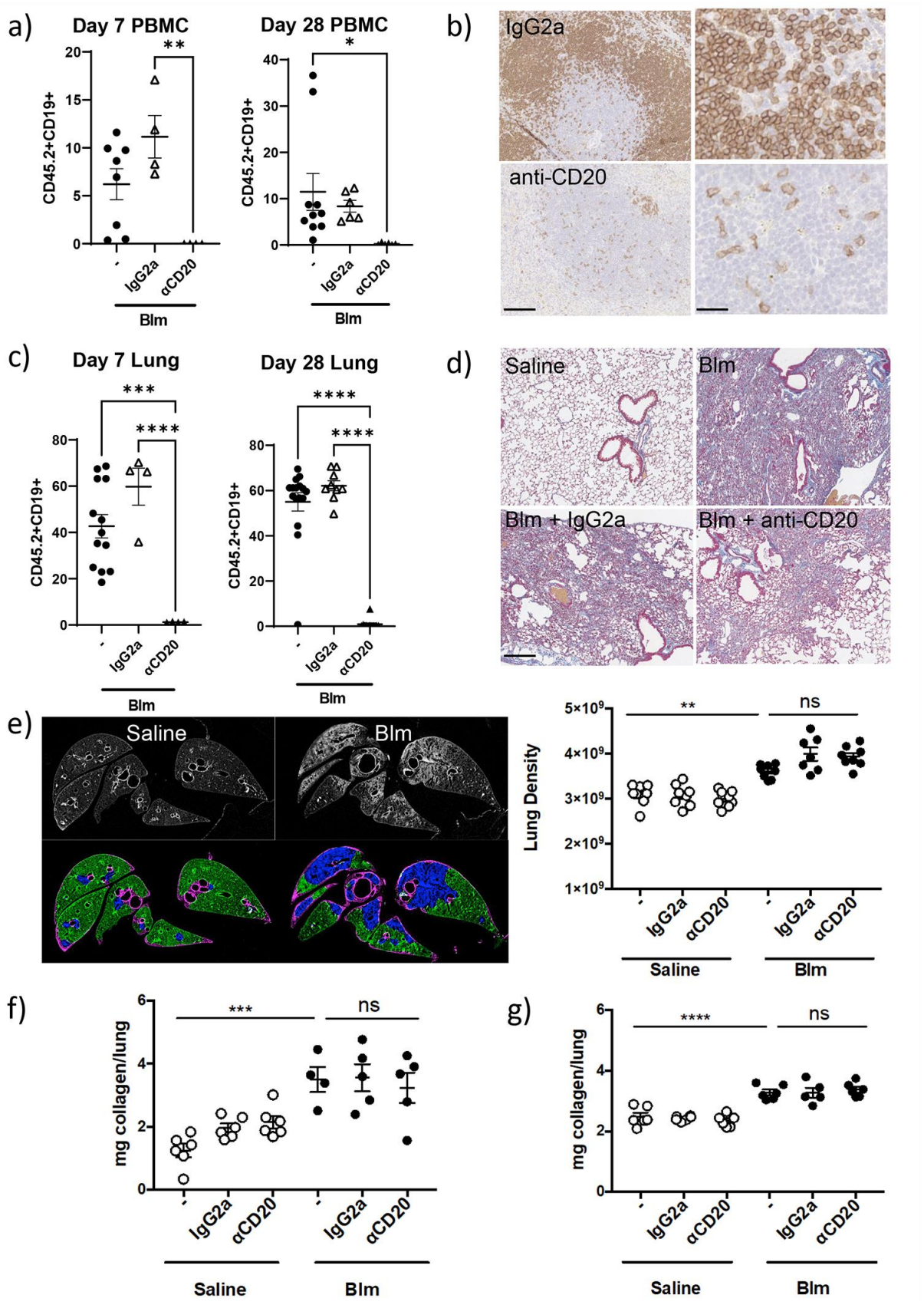
a)
Day 7 PBMC
Day 28 PBMC
CD45.2+CD19+
**
*
-
IgG2a
αCD20
Blm
b)
IgG2a
anti-CD20
c)
Day 7 Lung
Day 28 Lung
***
****
d)
Saline
Blm
Blm + IgG2a
Blm + anti-CD20
e)
Saline
Blm
Lung Density
ns
f)
mg collagen/lung
g)

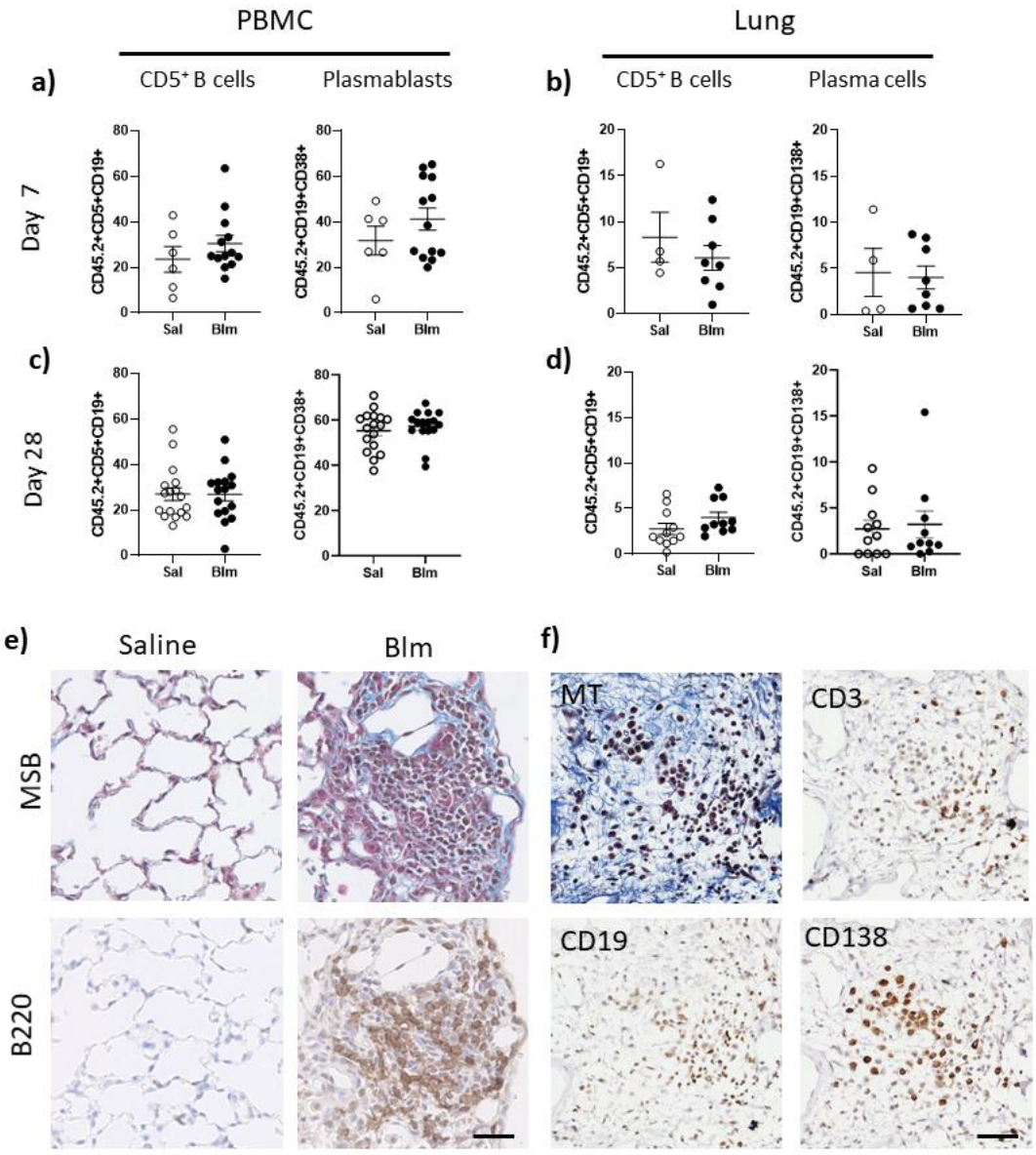
PBMC
Lung
a)
CD5⁺ B cells
Plasmablasts
b)
CD5⁺ B cells
Plasma cells
Day 7
CD45.2+CD5+CD19+
CD45.2+CD19+CD38+
CD45.2+CD19+CD138+
Sal
Blm
c)
d)
Day 28
e)
Saline
Blm
MSB
B220
f)
MT
CD3
CD19
CD138

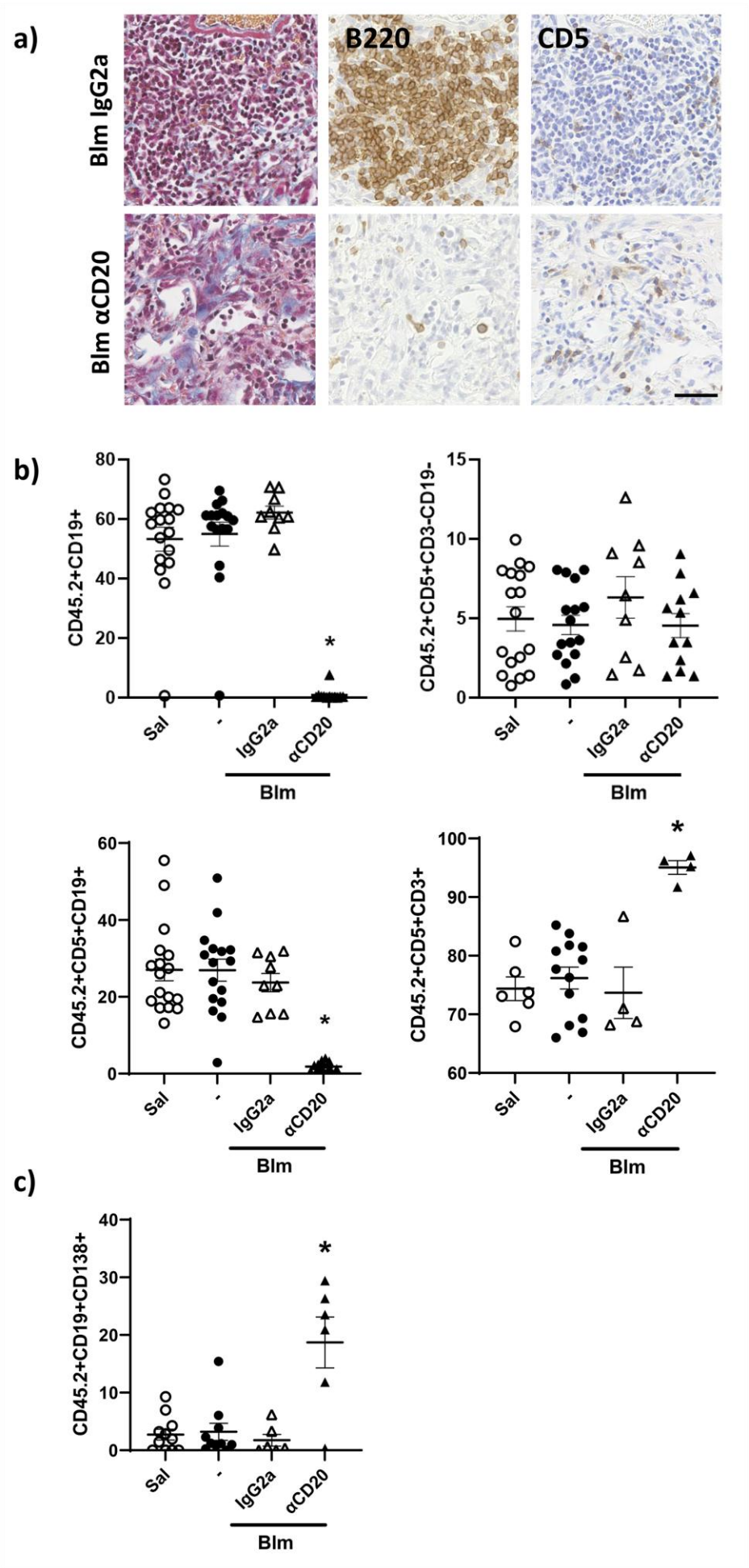
a)
Blm IgG2a
Blm αCD20
B220
CD5
b)
CD45.2+CD19+
CD45.2+CD5+CD3-CD19-
CD45.2+CD5+CD19+
CD45.2+CD5+CD3+
Sal
-
IgG2a
αCD20
Blm
c)
CD45.2+CD19+CD138+

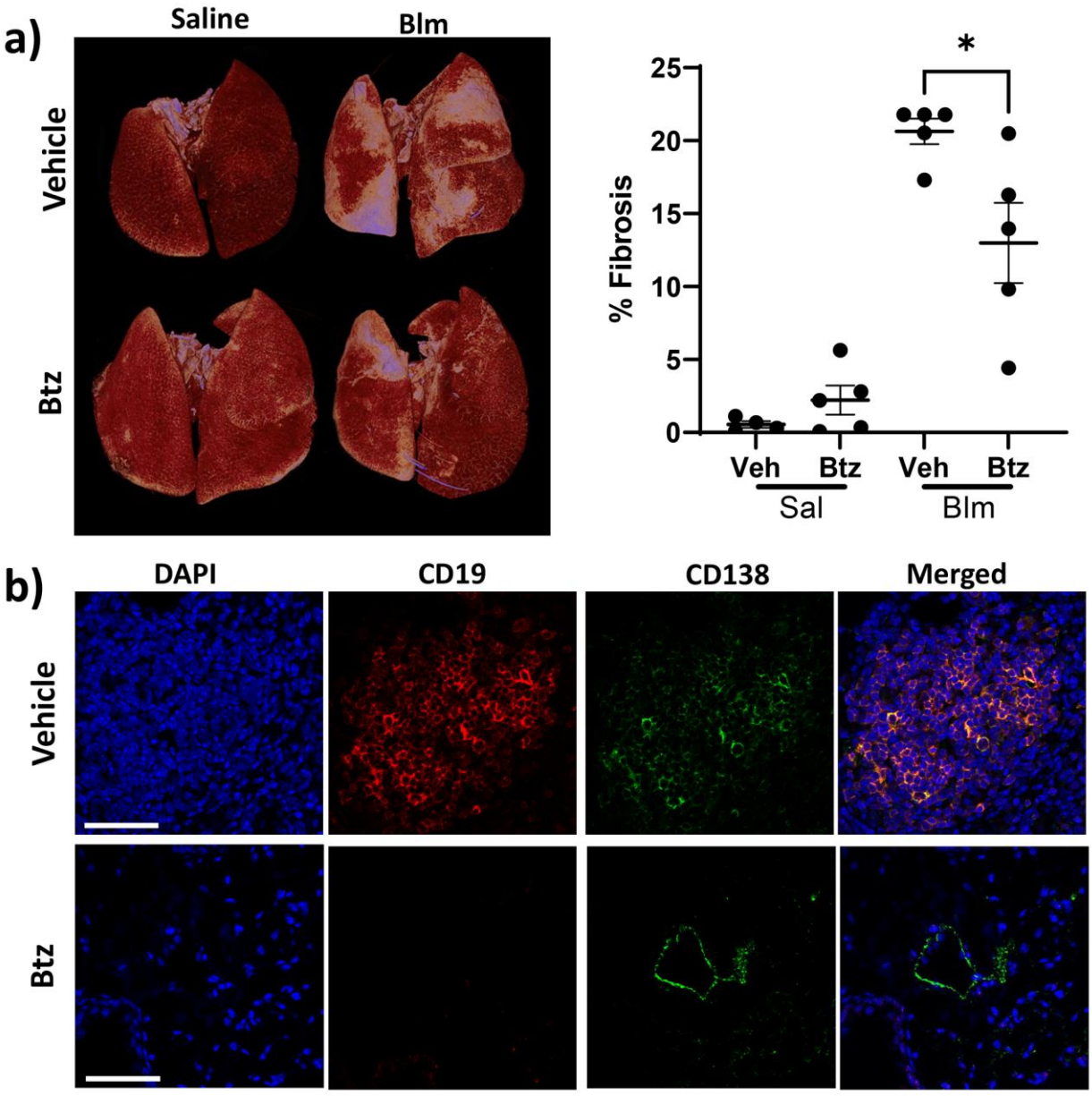
a)
Saline
Blm
Vehicle
Btz
% Fibrosis
25
20
15
10
5
0
*
Veh
Btz
Veh
Btz
Sal
Blm
b)
DAPI
CD19
CD138
Merged
Vehicle
Btz

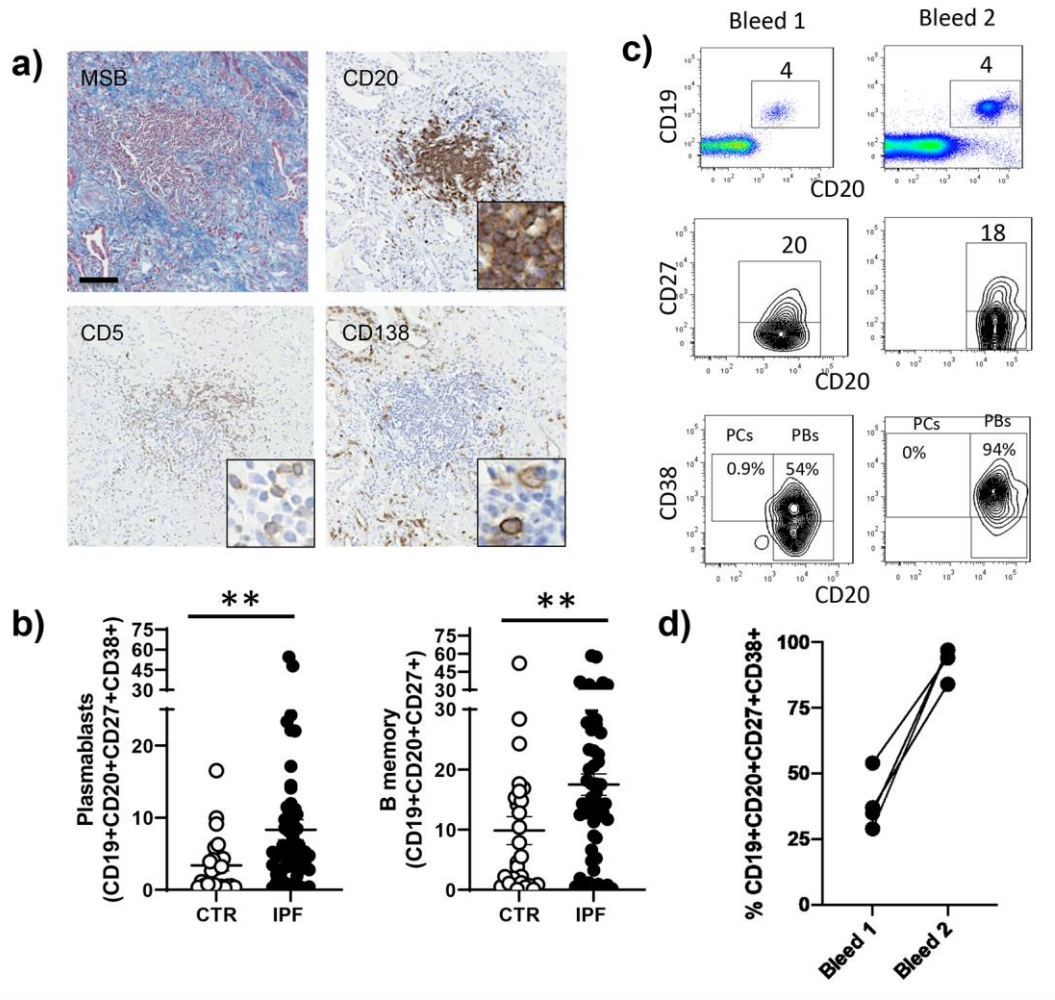
a)
MSB
CD20
CD5
CD138
b)
**
Plasmablasts (CD19+CD20+CD27+CD38+)
75
60
45
30
20
10
0
CTR
IPF
**
B memory (CD19+CD20+CD27+)
75
60
45
30
20
10
0
CTR
IPF
c)
Bleed 1
Bleed 2
CD19
CD20
4
4
CD27
CD20
20
18
CD38
CD20
PCs
PBs
0.9%
54%
PCs
PBs
0%
94%
d)
% CD19+CD20+CD27+CD38+
100
75
50
25
0
Bleed 1
Bleed 2

SUPPLEMENTARY SECTION

Plasma cell but not CD20-mediated B cell depletion protects from bleomycin-induced lung fibrosis

Cecilia M Prêle[1,2,*], Tylah Miles[1,*], David R Pearce[3], Robert J O'Donoghue[4], Chris Grainge[5,6], Lucy Barrett[1], Kimberly Birnie[1], Andrew D Lucas[1], Svetlana Baltic[1], Matthias Ernst[7], Catherine Rinaldi[8], Geoffrey J Laurent[1,2], Darryl A Knight[9], Mark Fear[1,5], Gerard Hoyne[1,9], Robin J McAnulty[3,#] and Steven E Mutsaers[1,2,#]

[1]Institute for Respiratory Health, The University of Western Australia, Nedlands WA Australia; [2]Centre for Cell Therapy and Regenerative Medicine, School of Biomedical Sciences, The University of Western Australia, Nedlands WA Australia; [3]Centre for Inflammation and Tissue Repair, Division of Medicine, University College London, London UK; [4]Department of Pharmacology and Therapeutics, University of Melbourne, VIC Australia; [5]Centre for Healthy Lungs, Hunter Medical Research Institute, University of Newcastle, Newcastle, NSW, Australia; [6]Dept of Respiratory and Sleep Medicine, John Hunter Hospital, Newcastle, NSW, Australia; [7]Olivia Newton John Cancer Research Institute and La Trobe University School of Cancer Medicine, Heidelberg, VIC Australia; [8]Centre for Microscopy Characterisation and Analysis, The University of Western Australia, Nedlands WA Australia; [9]Providence Health Care Research Institute, Vancouver, BC, Canada; [10]Burn Injury Research Unit, School of Biomedical Sciences, The University of Western Australia, Nedlands WA Australia; [11]The University of Notre Dame Australia, Fremantle WA Australia.

Supplementary Methods

Mouse lung and spleen dissociation and B cell phenotype analysis using flow cytometry.

Mouse lung tissue was harvested and dissected into 1-2 mm^3 pieces and incubated in 3 mL digestion medium consisting of 48 µg/mL Liberase™ (Roche), 0.1 mg/mL of DNase I in RPMI (Gibco® Life Technologies™) for 2 h at 37°C with constant shaking. The enzymatic activity within the digestion medium was neutralised with 4 mL RPMI/10% FCS and the lung cells collected by centrifuging at 300 g for 5 min.

Spleen cells were isolated by teasing the spleen with two needles and then washed in PBS, pH7.4. The isolated cells were resuspended in hypotonic cell lysis buffer (150 mM NH_4Cl, 10 mM $KHCO_3$, 0.1 mM Na_2EDTA, pH 7.4), incubated at room temperature (RT) for 7 min and then topped up with PBS to lyse the red blood cells. PBMC were isolated on a lymphoprep gradient using Cell SepMate Tubes (Stem Cell Technologies, UK) in accordance with the manufacturer's guidelines. All cells were resuspended and frozen in cyro-preservation medium (RPMI 50% FCS/10% DMSO).

Flow cytometry antibodies were diluted in a solution of 50% PBS and 50% BD Horizon Brilliant Stain™ (BD Biosciences, Franklin Lake, NJ, USA). Mouse PBMCs, lung and spleen cells were stained in 50 µL of the B cell antibody cocktail (Supplementary Table I) for 30 min on ice, washed twice in 100 µL of PBS/2% FCS and centrifuged at 300 g for 5 min. The cells were then resuspended in 200 µL of PBS/10% FCS and fixed with BD Cytofix/Cytoperm™ kit and stored at 4°C for up to 48 h. Flow cytometry was performed on BD LSRFortessa™ and analysis performed using FlowJo 10.3. B cell subsets were identified by flow cytometry; mature follicular B cells ($CD45.2^+CD19^+CD20^+$), B1 regulatory B cells ($CD45.2^+CD19^+CD20^-CD38^+CD5^+CD43^+$) and

plasma cells ($CD45.2^+CD19^+CD20^-CD138^+CD43^+CD38^+ CD27^+$) or plasmablasts ($CD45.2^+CD19^+CD20^+CD138^-CD43^+CD38^+ CD27^+$).

Histochemical and immunohistochemical analysis of fibrosis and immune cell infiltration in tissue. Mouse and human lung sections (3 µm) were dewaxed, and antigen retrieval performed in a pressure cooker by boiling slides in citrate buffer for 10 minutes and cooling. Endogenous peroxidase and non-specific antibody binding blocking steps were performed and then the tissues were incubated with primary antibody or appropriate control mouse or rabbit IgG overnight at 4°C. Tissue sections were washed three times in TRIS Buffered Saline (TBS) and then incubated in the appropriate biotinylated secondary antibody for 45 min followed by streptavidin/HRP for 30 min at RT. Immunolabelling was visualised by incubating tissue sections in 3,3′-Diaminobenzidine solution (DAB) (Sigma-Aldrich®) for up to 5 min. For CD138 staining of mouse lung tissue the Vector® M.O.M™ Immunodetection kit was used according to the manufacturer's instructions. For the detection of CD19 and CD138 by immunofluorescence the sections were incubated in the appropriate AF568- and AF488-conjugated secondary antibodies for 30 min at RT. The nuclei were visualised by incubating the section in 4',6-diamidino-2-phenylindole (DAPI) for 5 min at RT. Representative tissue sections were also stained for hematoxylin and eosin, Masson's trichrome or Martius scarlet blue (MSB) trichrome staining using a Tissue-Tek DRA autostainer (Sakura, Japan). Slides were imaged using either the Aperio ScanScope® XT (Leica Biosystems, Centre for Microscopy, Characterisation and Analysis, UWA) or Nanozoomer HT slide scanner (Hamamatsu, Japan; University College London).

Supplementary figure legends

Supplementary Figure 1. Gating strategy for mouse PBMCs and mouse lung cell flow cytometry analysis. Mouse PBMCs and dissociated lung cells were stained with a cocktail of fluorescently labelled monoclonal antibodies (mAbs) and analysed by flow cytometry. The leukocyte population was determined by gating $CD45.2^+$ cells. CD45 is a general leukocyte cell surface marker. Leukocytes were subsequently stratified into specific immune cell subsets. **a)** PCs were identified by selecting $CD19^+$ $CD3^-$ cells and then selecting $CD38^+$ and $CD138^+$ cells. **b)** B regulatory cells were identified by selecting $CD5^+$ and then $CD19^+$.

Supplementary Figure 2. Gating strategy for human white blood cell analysis using flow cytometry. Representative flow cytometry plots were shown for white blood cells from one control patient that was washed and stained with a cocktail of fluorescently labelled mAbs to distinguish T and B cell subsets. Lymphocytes were gated on FSC, and SSC properties and viable cells were gated and analysed for $CD3^+$ T cells and $CD19^+$ B cells. Mature B cells were identified as $CD19^+$ $CD20^+$ cells. These cells were then analysed for the presence of $CD20^+$ $CD27^+$ memory B cells (Bmem) and the Bmem cells were further analysed for the presence of $CD20^+$ $CD38^+$ plasmablasts (PBs).

Supplementary Figure 3. a) Low magnification image of a representative lung section from Blm + vehicle treated mice stained with H&E. The image shows areas of normal tissue and dense fibrosis, and multiple mononuclear cell aggregates are present within areas of fibrosis. Inset is enlarged in b) with a mononuclear cell aggregate (arrow). **b)** High magnification image of mononuclear cell aggregate contains $CD19^+CD138^+$ PCs (yellow). The isotype control shows no positive CD19 or CD138 staining. Scale bars = 100 µm.

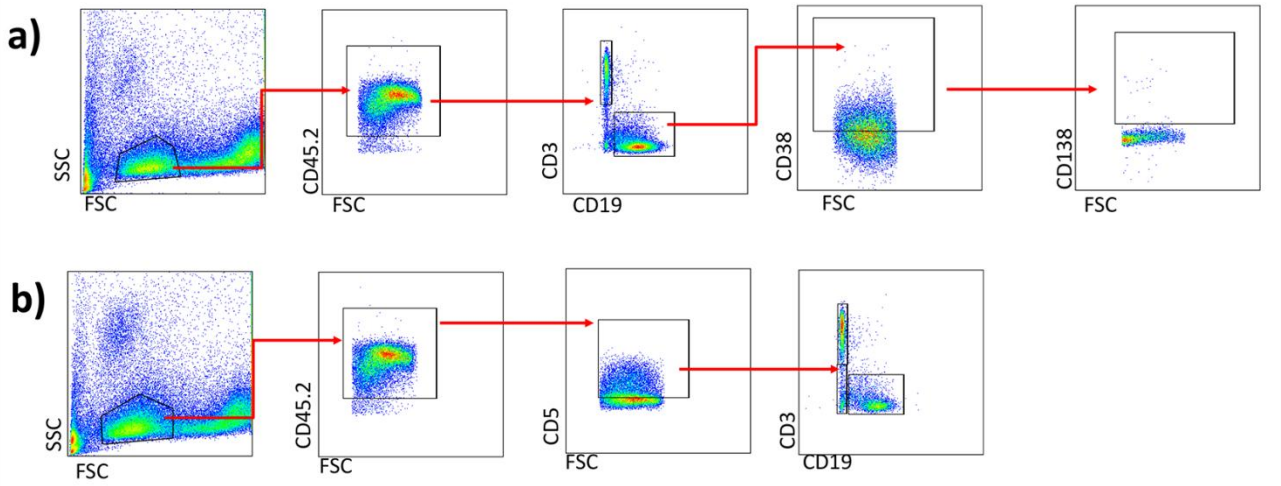
a)
SSC
FSC
CD45.2
FSC
CD3
CD19
CD38
FSC
CD138
FSC
b)
SSC
FSC
CD45.2
FSC
CD5
FSC
CD3
CD19

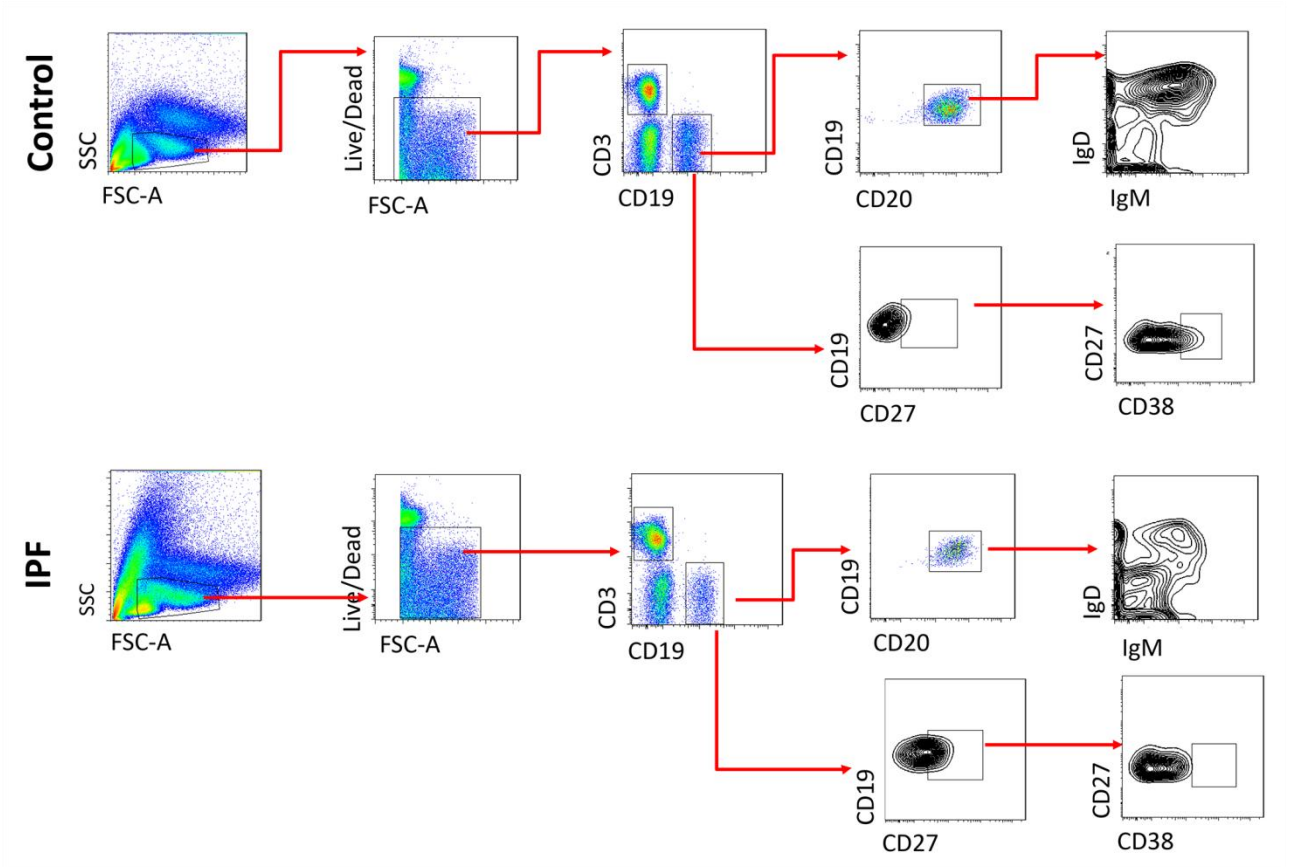
Control
SSC
FSC-A
Live/Dead
FSC-A
CD3
CD19
CD19
CD20
IgD
IgM
CD19
CD27
CD27
CD38
IPF
SSC
FSC-A
Live/Dead
FSC-A
CD3
CD19
CD19
CD20
IgD
IgM
CD19
CD27
CD27
CD38

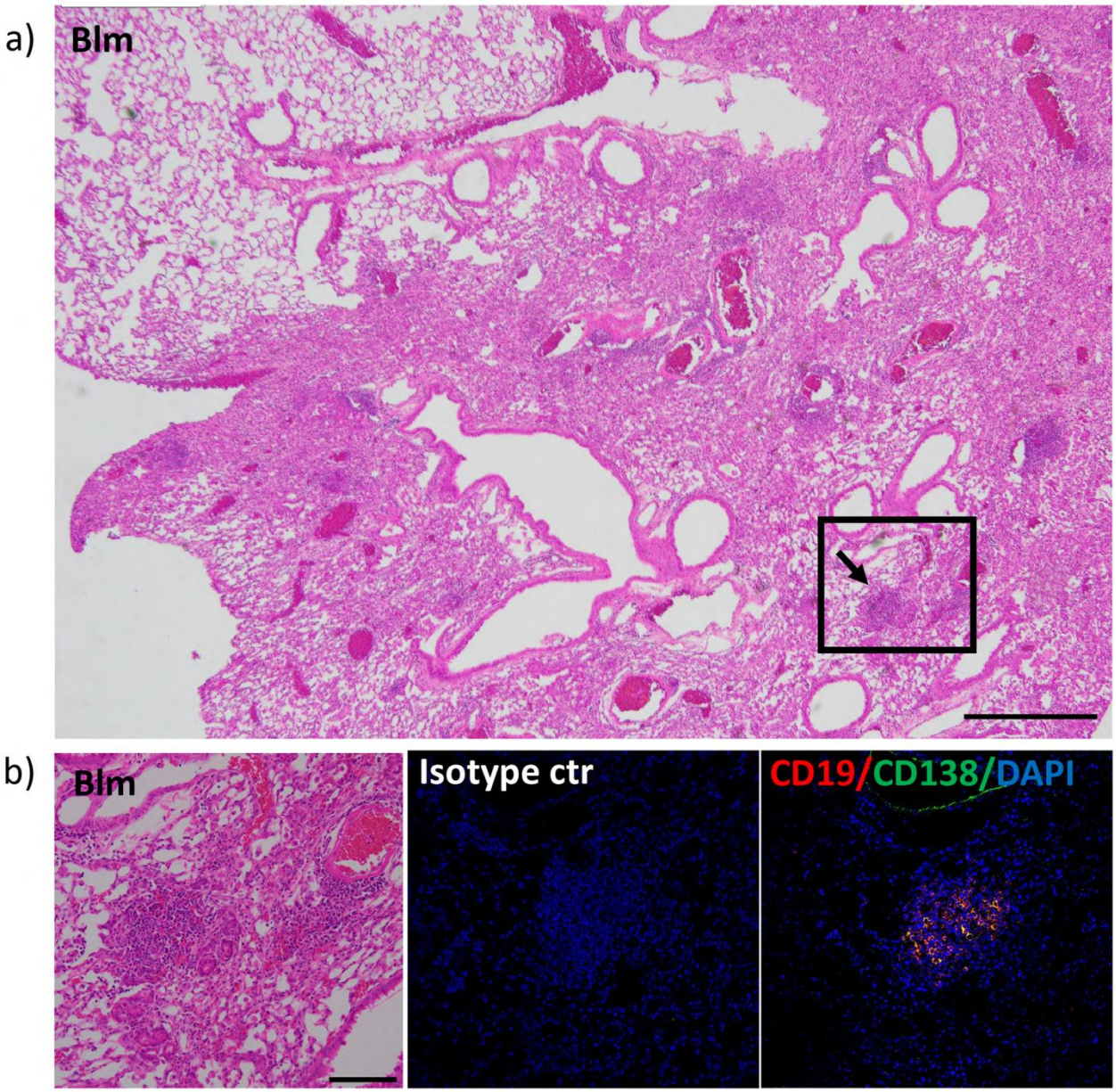
a)
Blm
b)
Blm
Isotype ctr
CD19/CD138/DAPI

Supplementary Table I

B Cell Panel – FACS Antibodies						
Marker	**Cell type**	**Fluorochrome**	**Conc**	**Filter**	**Catalogue Number**	**Manufacturer**
CD19	B cell	BUV395	4 µg/mL	355/379	563557	BD Horizon™ (Franklin Lakes,NJ)
CD3e	T cell	BV421	4 µg/mL	405/450	145-2C11	BD Horizon™
CD5	Breg	APC R700	1 µg/mL	640/730	565505	BD Horizon™
CD27	Activation marker	BV650	1 µg/mL	405/670	740491	BD OptiBuild™
CD20	B cell	PE	4 µg/mL	561/682	4287892	eBioscience
CD45.2	Total leukocyte	PerCP Cy 55	4 µg/mL	488/695	561096	BD Pharmingen™
CD38	Activation marker	FITC	2 µg/mL	488/530	558813	BD Pharmingen™
CD138	Plasma cell	BB515	4 µg/mL	405/525	564511	BD Horizon™
CD268	BAFF-R	BV711	1 µg/mL	405/710	742869	BD OptiBuild™